Electric-Field-Tunable Ferroelastic Control of Nonvolatile Resistivity and Ferromagnetic Switching in Multiferroic $La_{0.67}Ca_{0.33}MnO_3/[PbMg_{1/3}Nb_{2/3}O_3]_{0.7}[PbTiO_3]_{0.3}$ Heterostructures

Ming Zheng[1,2,*] and Ren-Kui Zheng[2]

[1]*Department of Materials Science and Engineering, Faculty of Engineering,*
National University of Singapore, Singapore 117574, Singapore
[2]*State Key Laboratory of High Performance Ceramics and Superfine Microstructure,*
Shanghai Institute of Ceramics, Chinese Academy of Sciences, Shanghai 200050, China

The electric-field-modulated nonvolatile resistivity and magnetization switching in elastically coupled $La_{0.67}Ca_{0.33}MnO_3$ films grown on (111)-oriented $0.7Pb(Mg_{1/3}Nb_{2/3})O_3$-$0.3PbTiO_3$ substrates is achieved through the ferroelastic effect. By taking advantage of the 180° ferroelectric and non-180° ferroelastic domain switching, we identify that such changes in order parameters stem from domain-switching-induced strain rather than accumulation or depletion of charge carriers at the interface. Specifically, the strong correlation between the ferroelastic strain and the magnetic field is manifested not only by the strain-tunable magnetoresistance effect but also by the magnetically manipulated strain effect, which is essentially driven by the electronic phase separation. These findings present a potential strategy for elucidating the essential physics of the ferroelastic-strain effect and delivering prototype devices for energy-efficient and nonvolatile information storage.

I. INTRODUCTION

A central goal of multiferroic heterostructures composed of a ferromagnetic thin-film layer and a ferroelectric polycrystalline or single-crystal layer lies in finding an energy-efficient way to achieve reversible and nonvolatile manipulation of magnetization and resistance by using a voltage across the ferroelectric layer, owing to its tremendous potential application in novel nonvolatile magneto-eletric electronic devices [1–9]. As one of the most fascinating ferromagnetic materials, perovskite manganites of $La_{1-x}Ca_xMnO_3$ have sparked a surge of research activities for decades due to various attractive physical phenomena, such as the colossal magnetoresistance effect, electroresistance, metal-to-insulator transition (MIT), charge and orbital ordering, and microscopic electronic phase separation (EPS) [i.e., the coexistence and competition between the ferromagnetic metallic (FMM) phase, charge-ordered antiferromagnetic insulating phase, and/or paramagnetic insulating (PMI) phase] [10–12]. Because of strong coupling of the lattice, spin, charge, and orbital degrees of freedom, the small evolution of lattice distortion and charge carriers near MIT can tip the subtle energy balance between the coexisting phases and, thus, eliminate the ferromagnetic domain inhomogeneity on the nanometer scale, thereby giving rise to remarkable variations in magnetic and electrical properties. Apart from lattice distortion and charge carriers, oxygen content [13], dead

layer at interface [14], and local Jahn-Teller-type lattice distortion [15], etc., are also demonstrated to have a strong impact on the EPS, making it rather difficult to obtain the intrinsic effects of lattice strain and charge carriers on EPS and MIT. In order to rule out the influences of these extrinsic variables on EPS and MIT, Sheng *et al.* [16], Wang and Gao [17], Zheng *et al.* [18], and Jiang *et al.* [19] fabricated $La_{1-x}Ca_xMnO_3$ ($x = 0.2, 0.25, 0.3$) thin films on the $(1-x)Pb(Mg_{1/3}Nb_{2/3})O_3$-$xPbTiO_3$ (PMN-PT) ferroelectric single-crystal substrates to elucidate the intrinsic coupling mechanisms between the lattice, charge, and spin degrees of freedom. However, the strain states in two absolutely converse polarization directions before and after 180° domain switching are equivalent, and the strain generated by the linear piezoeffect can vanish upon removing the control voltage, thus, failing to offer reversible and nonvolatile tunability of magnetic and electric order parameters [16,18,19]. Comparatively, the electric-field-induced interface charge effect (i.e., ferroelectric field effect) can be used to obtain nonvolatility of physical property switching only by decreasing the film thickness and/or by reducing the sample temperature, due to a small screening length of applied voltage within several unit cells and/or a large number of charge carrier in the films, respectively [18,20]. Fortunately, recent experiment studies on $Co_{40}Fe_{40}B_{20}$/PMN-PT(001) [5], Fe_3O_4/PMN-PT(110) [21], $Bi_{0.95}Mn_{0.05}FeO_3$/PMN-PT(111) [22], and VO_2/PMN-PT(111) [23] heterostructures have demonstrated that the nonvolatile and reversible modulation of lattice strain and physical properties has been observed via

*msezhengm@nus.edu.sg

two stable and reversible remnant in-plane strain states of the PMN-PT substrates, which originate from the non-180° ferroelastic domain switching [24,25]. Despite the efforts devoted to *in situ* dynamical manipulation of lattice-sensitive physical parameters of $La_{1-x}Ca_xMnO_3$ films, the impacts of the non-180° ferroelastic domain switching on the lattice strain, electronic transport, and magnetic properties are still missing and remain unaddressed. Actually, an in-depth understanding of certain important issues regarding the $La_{1-x}Ca_xMnO_3$/PMN-PT heterostructures, such as the relative importance of the electric-field-induced strain effect and interface charge effect, the evolution of the film strain against the ferroelectric or ferroelastic domain switching of the underlying substrates, the effects of the in-plane tensile strain on EPS, and how the ferroelastic strain interacts with the magnetic field will help to elucidate the essential physics of manganites and ferroelastic effects, which is undoubted also important to design nonvolatile magnetoelectric electric devices.

Motivated by these unaddressed questions, we grow epitaxial $La_{0.67}Ca_{0.33}MnO_3$ (LCMO) thin films on (111)-oriented $0.7Pb(Mg_{1/3}Nb_{2/3})O_3\text{-}0.3PbTiO_3$ ferroelectric single-crystal substrates and realize non-180° ferroelastic domain switching by applying an electric field with appropriate magnitude (less than the coercive field of PMN-PT). The ferroelastic polarization switching of the PMN-PT substrate enables the expansion of film in-plane lattice, which, in turn, robustly modulates the Curie temperature T_C, electronic transport, and ferromagnetism, as well as the EPS of the LCMO film. We also pay particular attention to the mutual interactions between the ferroelastic strain and the magnetic field and the nonvolatile resistance and magnetization tunability of the films using the ferroelastic effects of the PMN-PT substrates.

II. EXPERIMENTAL DETAILS

LCMO films are prepared on one-side polished and (111)-oriented PMN-PT commercial single-crystal substrates (Hefei Kejing Materials Technology Co. Ltd., People's Republic of China) by pulsed-laser deposition. The detailed growth method can be referred to our earlier work [12,26]. The film thickness is determined to be approximately 45 nm, as illustrated by the cross-sectional backscattered electron image (not shown here). The atomic-force-microscopy measurement reveals that the film has a flat surface with a root-mean-square roughness $R_q \sim 1.1$ nm, as depicted in Fig. 1(d). The local ferroelectric responses of PMN-PT substrates are analyzed via piezoresponse force microscopy (PFM) using a Dimension V (Veeco) scanning probe microscope. The crystal structure of the film and the epitaxial relationship of the film with respect to the underlying substrate are characterized using a high-resolution Bruker D8 Discover x-ray diffractometer (XRD) attached with a four-bounce Ge(220) monochromator and Cu $K_{\alpha 1}$ radiation
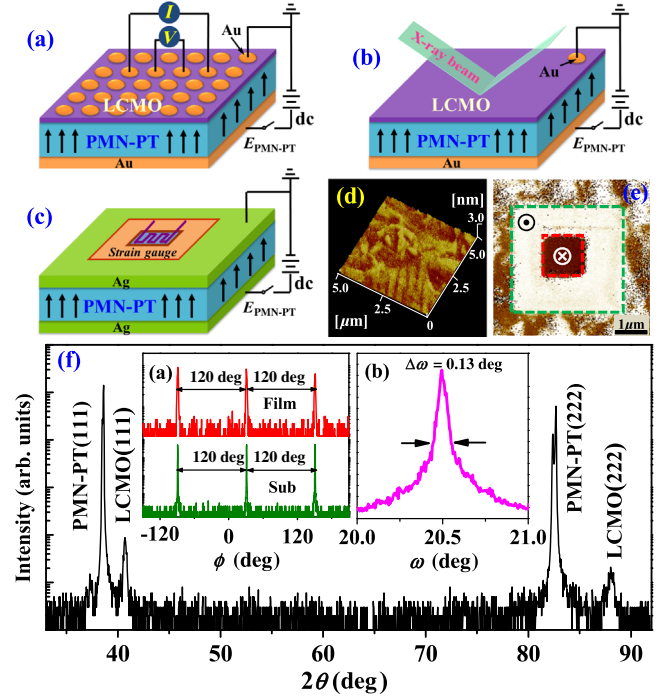

FIG. 1. (a)–(c) Schematic of the experimental setups for *in situ* measurements of film resistance, out-of-plane strain, and in-plane strain of the PMN-PT substrate, respectively. (d),(e) show the surface morphology of the LCMO film and out-of-plane PFM image of the PMN-PT substrate, respectively. (f) XRD θ-2θ scan of the LCMO/PMN-PT structure. Inset (a): XRD ϕ scans taken on the LCMO(101) and PMN-PT(101) diffraction peaks. Inset (b): XRD rocking curve taken on the LCMO(111) diffraction peak.

($\lambda = 1.5406$ Å), and a high-resolution transmission electron microscope (TEM, Tecnai G2 F20 S-Twin), respectively. The ferroelectric poling, 180° ferroelectric, and non-180° ferroelastic domain switching are conducted by applying a proper dc electric field across the PMN-PT substrate along the [111] crystal direction through the conducting LCMO film and the sputtered bottom Au electrode (approximately 120 nm) using a Keithley 2410 sourcemeter. The film resistivity is measured using the standard four-probe method on the physical property measurement system (PPMS-9, Quantum Design). Magnetic data are recorded by a superconducting quantum-interference device magnetometer (MPMS XL-5, Quantum Design) with the magnetic field applied parallel to the film plane. Prior to the measurements, we apply a sufficiently large dc electric field of $E = 10$ kV/cm across the LCMO/PMN-PT heterostructure for 20 min to ensure the PMN-PT substrate is absolutely positively poled (i.e., the electric dipole moments point towards the LCMO film denoted by P_r^+).

III. RESULTS AND DISCUSSION

Figure 1(f) shows the XRD θ-2θ scan pattern for the as-grown LCMO/PMN-PT heterostructure in the P_r^+ state.

The LCMO film is highly (111) oriented, and no diffraction peaks indicative of other impurities are observed, suggesting the single-phase nature of the deposited film. The XRD rocking curve [see inset (b) of Fig. 1(f)] taken on the LCMO(111) diffraction peak has a full width at half maximum of 0.13°, implying good crystalline quality of the LCMO film. In order to establish the in-plane epitaxial relationship of the film with respect to the substrate, we perform XRD ϕ scans, which are taken on the (101) diffraction peaks of the LCMO film and the PMN-PT substrate, respectively, and present the results in the inset (a) of Fig. 1(f). Obviously, two sets of trifold symmetrical diffraction peaks recurring every 120° are found at the same azimuthal ϕ angle, firmly proving the "cube-on-cube" epitaxial nature of the LCMO film on the PMN-PT substrate. A schematic diagram of the in-plane atomic arrangements for the LCMO unit cell on the PMN-PT substrate is shown in Fig. S1 of the Supplemental Material [27]. The out-of-plane lattice spacing d_{111} of the LCMO film (2.222 Å) is somewhat smaller than that of the LCMO bulk value (2.229 Å). This result hints that the LCMO film suffers an out-of-plane compressive strain (−0.31%) and an in-plane tensile strain, which corresponds to the smaller lattice constants of the LCMO bulk ($a \sim b \sim c \sim 3.86$ Å) [28,29] than those of the PMN-PT substrate ($a \sim b \sim c \sim 4.02$ Å). To further probe into the in-plane orientation relationship of the LCMO/PMN-PT heterostructure, a high-resolution TEM image is measured at the interface of the structure shown in the Supplemental Material [27] Fig. S2(a), where two sets of clear lattice fringes of the LCMO film (PMN-PT substrate) with lattice spacings of 0.38 nm (0.4 nm) for the family of (001) planes and 0.27 nm (0.28 nm) for the family of (110) planes are displayed, respectively. This image also discloses an in-plane epitaxial arrangement of LCMO(001)/PMN-PT(001) and LCMO(110)/PMN-PT(110), which is fully consistent with the XRD results. The epitaxial relationship can be further corroborated by the selected-area electron-diffraction pattern [see the Supplemental Material [27] Fig. S2(b)] taken from a selected interface area of the heterostructure, where two appreciable sets of diffraction patterns are collected, due to the disparity in lattice parameters between the PMN-PT and the LCMO. All the above microscopic characterizations clearly establish the high degree of crystallinity and smooth interface of the LCMO film, making it greatly promising to achieve strong mechanical coupling at the interface for the LCMO/PMN-PT heterostructure.

Figure 2(a) shows the *in situ* electric field tuning of the resistivity of the LCMO film with different voltage-switching pathways at room temperature using the schematic of the experimental setups depicted in Fig. 1(a). Upon cycling a sufficiently large bipolar electric field with an amplitude of $E = 8.5$ kV/cm, a butterflylike resistivity versus electric field curve (blue) is observed
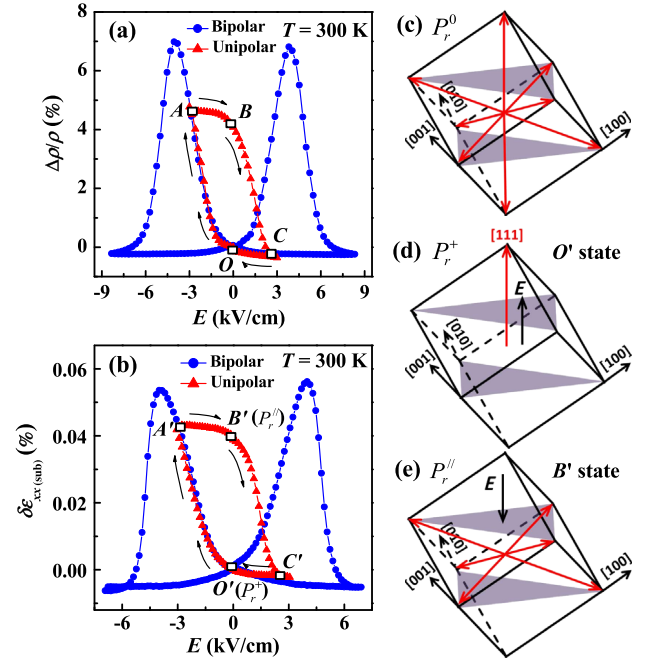

FIG. 2. (a),(b) show electric-field-induced relative resistivity evolution of the LCMO film and in-plane strain of the PMN-PT substrate as a function of bipolar and unipolar E applied across the PMN-PT at $T = 300$ K. (c)–(e) Schematic of the polarization vectors in the rhombohedral phase under the P_r^0, P_r^+, and $P_r^{//}$ states for the PMN-PT, respectively.

with a relative resistivity change ($\Delta\rho/\rho$) of 7% at room temperature. Here, $\Delta\rho/\rho$ is defined as $\Delta\rho/\rho = [\rho(\text{E}) - \rho(0)]/\rho(0)$. An in-plane strain measurement using a strain gauge [see Fig. 1(c)] reveals that the electric-field-induced in-plane strain $\delta\varepsilon_{xx(\text{sub})}$ versus E curve of the PMN-PT substrate has a similar butterflylike pattern [see Fig. 2(b)] as that of the $\Delta\rho/\rho$ versus E curve of the LCMO film, intuitively demonstrating the strain-induced nature of the resistivity evolution and, thus, precluding the possible charge-mediated coupling mechanism in this system. It has been reported that the poling-induced strain microscopically arises from the rearrangement of ferroelectric domain structures in the PMN-PT substrates, thus, influencing the electrical and magnetic properties of the heterostructures [7,30]. Accordingly, we measure the PFM image of the PMN-PT substrate during ferroelectric domain switching to understand the evolution of strain with domain structures and show the result in Fig. 1(e). As can be seen in Fig. 2(c), the spontaneous polarization vectors of the PMN-PT substrate randomly point along the eight body diagonals of the pseudocubic cell with rhombohedral symmetry at room temperature when the PMN-PT is in the initial or unpoled state (denoted by P_r^0), which leads to a mixture of ferroelectric domains [see Fig. 1(e)]. When applying a voltage of −10 V on the tip, both ferroelectric domain switching (180°) and ferroelastic domain switching (109° and 71°) occur, and all the polar vectors rotate upward in

the poled area (green box), pointing along the [111] direction (denoted by P_r^+) [Fig. 2(d)]. Subsequently, when a dc voltage of $+10$ V is applied in a smaller area (red box) inside of the green box, all the polar vectors previously pointing along the [111] direction are reversed and point downward (denoted by P_r^-). In this symmetric bipolar electric field scenario, the 180° polarization switching fails to induce a visible variation in the resistivity states due to the strain equivalence in these two domain structures (i.e., P_r^+ and P_r^- states). However, upon cycling an appropriate unipolar E (e.g., $E = 3 \text{kV/cm} < E_{C(\text{PMN-PT})}$), a hysteretic response of $\Delta\rho/\rho$ to E is observed, similar to the findings on the Fe_3O_4/PMN-PT(011) [21] and VO_2/PMN-PT(111) [23] heterostructures. Meanwhile, a hysteretic looplike $\delta\varepsilon_{xx(\text{sub})} \sim E$ curve (red) is also found for $E < E_{C(\text{PMN-PT})}$ in Fig. 2(b), further confirming that it is the strain transferred from the PMN-PT substrate that determines the resistivity evolution. One can see that the in-plane strain of the PMN-PT substrate will be maintained in the absence of externally applied electric field, hinting at the existence of a metastable state of the ferroelectric domains due to non-180° domain switching in the vicinity of $E_{C(\text{PMN-PT})}$ [24,25]. Namely, once applying a small negative electric field $E = -3$ kV/cm($|E| < E_{C(\text{PMN-PT})}$) to the positively poled PMN-PT substrate (i.e., O' state), the ferroelectric domains may rotate from the [111] to the [1-11], [11-1], [-111], [1-1-1], [-1-11], or [-11-1] directions, and, thus, the polarization undergoes 71° and/or 109° ferroelastic switching from the upward to the in-plane direction (denoted by $P_r^{//}$). Consequently, an in-plane tensile strain is induced in the PMN-PT substrate, corresponding to the evolution of the strain state from O' to A' in Fig. 2(b). Once the $E = -3$ kV/cm is removed, the in-plane strain remains largely unchanged due to the stability of the remnant in-plane polarization of the PMN-PT; namely, the strain state changes from A' to B', but it does not return to O'. Under such circumstance, the resistivity of the LCMO film accordingly evolves from O to A then to the B state. Afterwards, with the application of $E = +3$ kV/cm, the in-plane polarization is switched back to the upward direction, releasing the previously induced remnant in-plane tensile strain, which is also reflected by the evolution of the strain state from the B' to the C' state. After the $E = 3$ kV/cm electric field is turned off, the in-plane strain returns to the O' state. Accordingly, the film resistance recovers to the initial value (i.e., O state). These two stable and reversible remnant resistivity states (O and B states) will facilitate the realizing of nonvolatile resistivity switching by reversing the applied electric field near $E_{C(\text{PMN-PT})}$.

To achieve greater ferroelastic control of the resistivity of the LCMO film, we record the resistivity modulation by applying appropriate voltages at several fixed temperatures, as stated in Fig. 3(a). Upon decreasing the temperature
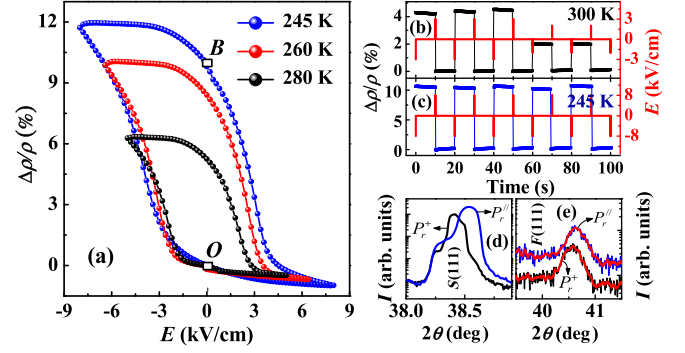

FIG. 3. (a) Resistivity hysteresis loops at temperatures as stated. (b),(c) show the nonvolatile resistivity switching of the LCMO film by a pulse electric field at $T = 300$ and 245 K, respectively. (d),(e) show XRD θ-2θ scans for the PMN-PT(111) substrate and the LCMO(111) film under the P_r^+ and $P_r^{//}$ states, respectively.

from $T = 300$ to 245 K, a larger electric field is needed to cycle a sufficiently large $\Delta\rho/\rho \sim E$ hysteresis loop, due to the enhancement of the coercive field of the PMN-PT substrate at low temperatures. The two reversible resistivity states (O and B states) at $T = 245$ K correspond to two stable and switchable remnant strain states with the upward (P_r^+) and in-plane ($P_r^{//}$) polarization directions, respectively, as shown in Figs. 2(d) and 2(e). In situ XRD measurements are carried out to investigate the structural evolution of the LCMO/PMN-PT heterostructure using the experimental setups in Fig. 1(b). As can be seen in Figs. 3(d) and 3(e), after the polarization direction is switched from the P_r^+ state to the $P_r^{//}$ state, both the PMN-PT(111) and LCMO(111) diffraction peaks shift to higher Bragg angles, indicating a contraction along the out-of-plane direction accompanied by an effective in-plane expansion of both the PMN-PT and the LCMO. The reduced out-of-plane compressive strain can be calculated as 0.135% and 0.333% for the LCMO film and the PMN-PT substrate, respectively. Using the Poisson relation $\delta\varepsilon_{zz} = -2\nu/(1-\nu)\delta\varepsilon_{xx}$ [31], and $\nu = 0.35$ and 0.5 for the LCMO [12] and the PMN-PT [32], the enhanced in-plane tensile strain is estimated to be 0.125% and 0.166%, respectively. Thus, the effective strain transfer coefficient α is approximately 75% ($\alpha = \delta\varepsilon_{xx(\text{LCMO})}/\delta\varepsilon_{xx(\text{PMN-PT})}$), disclosing good transferring of the induced ferroelastic strain from the PMN-PT substrate to the LCMO film. Using this ferroelastic-strain effect, we realize the electric-field-controlled reversible and nonvolatile resistivity switching of 4% and 10% for the LCMO/PMN-PT heterostructure at room temperature and $T = 245$ K, respectively, as shown in Figs. 3(b) and 3(c). It is interesting that multiple metastable resistivity states can be generated by applying proper electric field pulses at room temperature, which is closely related to the relative proportion of in-plane polarization vectors during switching [7,23]. For example, the nonvolatile resistivity switching of 2% can be achieved

by precisely applying a sequence of $E = \pm 2$ kV/cm pulses. The domain-engineered ferroelastic switching offers an energy-efficient way to design prototype devices for nonvolatile information storage. We note that the resistivity change shows a slight decay over the approximately 10-s period of measurement after application of an electric field pulse in Figs. 3(b) and 3(c), probably due to the stress-release process in the PMN-PT single crystal. The electric-field-induced ferroelastic domain switching produces stresses in the PMN-PT crystal, which can be released by the introduction of strains in the crystal. This process needs some time to reach equilibrium. The strain relaxation process will be simultaneously transferred to the overlying LCMO film, leading to the decay of the resistivity evolution.

To tap into the effect of the ferroelastic strain on the transport behavior, we measure the temperature dependence of the resistivity under magnetic fields for the LCMO film under both the out-of-plane (P_r^+) and in-plane ($P_r^{//}$) polarization directions, respectively. As shown in Fig. 4(a), associated with the polarization switching from the P_r^+ to $P_r^{//}$ state, a significant enhancement in the resistance and a visible suppression of Curie temperature T_C are observed with or without the application of an external magnetic field, implying that the in-plane tensile strain ($\delta \varepsilon_{xx(\text{LCMO})} = 0.125\%$) stabilizes the PMI phase but disfavors the FMM phase. Moreover, whether the LCMO film is at $H = 0, 1, 3,$ or 6 T, the resistivity curves of the P_r^+ state ($\boldsymbol{O}$) have similar patterns as those of the next consecutive

P_r^+ state after a cycle ($\boldsymbol{O} \rightarrow \boldsymbol{B} \rightarrow \boldsymbol{O}$), exhibiting electrically stable, reversible, and nonvolatile ferroelastic strain of the PMN-PT substrate. In order to understand the correlation between the ferroelastic strain and the EPS further, we fit the resistivity of the LCMO film throughout the entire temperature range using the equation $\rho = f_{\text{FMM}} \rho_{\text{FMM}} + (1 - f_{\text{FMM}}) \rho_{\text{PMI}}$ based on the phenomenological model describing the EPS [33], where f_{FMM} and $(1 - f_{\text{FMM}})$ are the volume fractions of the FMM phase and the PMI phase, respectively. Here, the temperature dependence of f_{FMM} obeys a two-energy-level Boltzmann distribution and can be expressed as $f_{\text{FMM}} = 1/\{1 + \exp[U_0/k_B(1/T_C^{\text{mod}} - 1/T)]\}$ [33]. ρ_{FMM} and ρ_{PMI} are the resistivities of the FMM phase and the PMI phase and can be expressed as $\rho_{\text{FMM}}(T) = \rho_0 + AT^2 + BT^5$ and $\rho_{\text{PMI}}(T) = C \exp[(T_0/T)^{1/4}]$, respectively [33]. The red solid lines in Fig. 4(a) are the fitted results, which agree with the experimental data quite well. Using the fitting parameters listed in Table I of the Supplemental Material [27], we obtain the temperature dependence of f_{FMM} under various magnetic fields for the LCMO film at two different in-plane strain states [Fig. 4(b)]. Accompanied by the polarization switching from the P_r^+ to $P_r^{//}$ state, f_{FMM} is dramatically reduced near T_C. Furthermore, it can be found that f_{FMM} is most sensitive to the ferroelastic strain at $H = 0$ T, where Δf_{FMM} [$\Delta f_{\text{FMM}} = f_{\text{FMM}}(P_r^{//}) - f_{\text{FMM}}(P_r^+)$] shows the negative maximum (21%) [see inset of Fig. 4(b)]. Apparently, the effects of the ferroelastic strain on f_{FMM} are strongly dependent on the magnetic field. It is, thus, speculated that the magnetic field will manipulate the ferroelastic-strain effect by adjusting the relative strength of EPS.

In order to quantify the response of the relative strength of EPS to the magnetic field, we plot the ferroelastic-strain tunability of resistivity (β_ρ) as a function of the magnetic field at several fixed temperatures as stated and show the results in Fig. 4(c). Here, β_ρ is defined as $\beta_\rho = \{[\rho(P_r^{//}) - \rho(P_r^+)]/\rho(P_r^+)\}/\delta\varepsilon_{xx(\text{LCMO})}$. In the vicinity of T_C, e.g., $T = 245$ K, β_ρ initially increases with increasing H but drops with further H increase, with a maximal value of 183 at $H = 1.2$ T. This result means that a change of in-plane strain by 0.125% leads to a maximal relative change in the resistance by 22.9% for the LCMO film at $H = 1.2$ T and $T = 245$ K. A similar strong response of resistance modulation to the stress field is also observed in the SmSe rare-earth chalcogenide thin films [34]. This phenomenon suggests that the LCMO film shows the maximal EPS tendency at $H = 1.2$ T for $T = 245$ K, indicative of the extreme sensitivity of the EPS to the ferroelastic strain. Because of the subtle balance and the minimum energy difference between the coexisting FMM and PMI phases near T_C, a small external perturbation (e.g., ferroelastic strain) can easily convert the FMM phase into the PMI phase, causing a pronounced resistivity
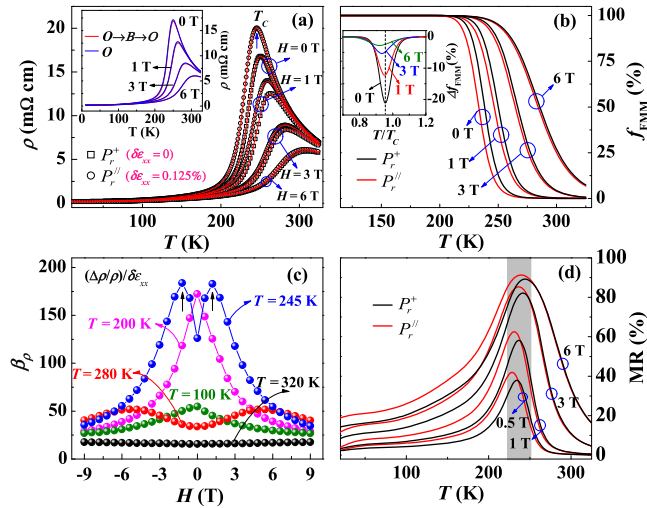

FIG. 4. Temperature dependence of the resistivity (a), f_{FMM} (b), and MR (d) for the LCMO film under magnetic fields as stated for the P_r^+ and $P_r^{//}$ states, respectively. Red solid lines in (a) are the fitted results. Inset in (a) shows the resistivity curves for two consecutive P_r^+ states ($\boldsymbol{O}$ and $\boldsymbol{O} \rightarrow \boldsymbol{B} \rightarrow \boldsymbol{O}$). Inset in (b) shows Δf_{FMM} versus T/T_C under $H = 0, 1, 3,$ and 6 T for the LCMO film. (c) $(\Delta\rho/\rho)/\delta\varepsilon_{xx}$ versus H curves for the LCMO film at temperatures as stated.

variation. Similarly, at $T = 280$ K, the film shows the maximum EPS at $H = 4.8$ T, as manifested by the largest $\beta_\rho \sim 51.6$ at $H = 4.8$ T. Nevertheless, the isothermal β_ρ decreases monotonically with increasing H for $T < T_C$ (e.g., $T = 200$ and 100 K) but increases gently with increasing H for $T > T_C$ (e.g., $T = 320$ K), substantiating that the relative strength of EPS is suppressed by H for $T < T_C$ but enhanced by H for $T > T_C$. The magnetically tunable ferroelastic-strain effect is microscopically a consequence of the magnetic-field-induced evolution in the relative strength of EPS and demonstrates the effectiveness of magnetic field tunability of EPS. The strong coupling of the ferroelastic strain and the magnetic field is reflected not merely by the magnetically manipulated strain effect but also by the strain-tunable magnetoresistance (MR) effect. The latter effect is presented in Fig. 4(d), where the MR versus T curves for the P_r^+ and $P_r^{//}$ states have a crossover near T_C at any fixed H, showing opposing effects of the ferroelastic strain on MR above and below T_C. At low temperatures, the FMM phase dominates over the PMI phase. After the polarization state is switched from the P_r^+ to the $P_r^{//}$ state, the in-plane tensile strain disfavors the FMM phase and, thus, enhances the relative strength of EPS, thereby enabling a noticeable increase in MR. For example, the relative change in MR, ΔMR/MR $= [\mathrm{MR}(P_r^{//}) - \mathrm{MR}(P_r^+)]/\mathrm{MR}(P_r^+)$, reaches 32% at $T = 25$ K for $H = 6$ T. In contrast, at high temperatures, the PMI phase dominates over the FMM phase. The in-plane tensile strain leads to the decrease in MR, caused by the suppression of the relative strength of EPS. These data discussed above clearly prove that the ferroelastic strain strongly interacts with the magnetic field, which is essentially mediated by the EPS.

The ferroelastic strain does not only efficiently modify the resistivity and MR but also lead to the considerable evolution of magnetic properties of the LCMO film. Figure 5(a) presents the temperature dependence of the zero-field-cooled (ZFC) and field-cooled (FC) magnetization for the LCMO/ PMN-PT structure under the P_r^+ and $P_r^{//}$ states, respectively. We find that the in-plane tensile strain suppresses the in-plane magnetization whether from the FC curve or from the ZFC one, especially at low temperatures, as clearly shown in Fig. 5(b). Here, ΔM is defined as $\Delta M = M(P_r^+) - M(P_r^{//})$. This ferroelastic-strain-induced reduction of the ferromagnetism is further corroborated by the magnetic hysteresis loops measured at $T = 10$ K for the P_r^+ and $P_r^{//}$ states [see inset of Fig. 5(a)]. The figure of merit that characterizes the effectiveness of the strain tunability of magnetization can be expressed as $\beta_M = \{[M(P_r^+) - M(P_r^{//})]/M(P_r^+)\}/\delta\varepsilon_{xx(\mathrm{LCMO})}$. Several selected β_M values are calculated and plotted against temperature shown in the inset of Fig. 5(b). Remarkably, β_M has a maximum value of 1768 at $T = 245$ K, close to T_C, signaling the maximal sensitivity of the magnetization to lattice strain at around T_C.
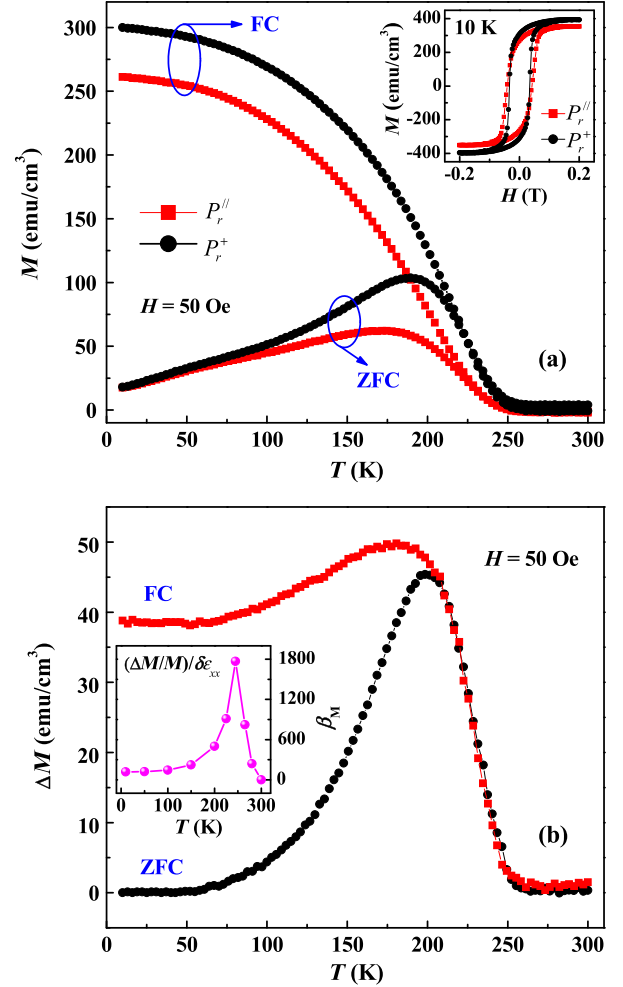

FIG. 5. Temperature dependence of ZFC and FC magnetization (a) and ΔM (b) for the LCMO film under the P_r^+ and $P_r^{//}$ states, respectively. Inset in (a) shows the magnetic hysteresis curves at $T = 10$ K for the LCMO film under the P_r^+ and $P_r^{//}$ states, respectively. Inset in (b) shows the $(\Delta M/M)/\delta\varepsilon_{xx}$ versus T curve for the LCMO film.

This finding means that an evolution of in-plane strain by 0.125% results in a maximal relative change in the magnetization by 221% for the LCMO film at $H = 50$ Oe and $T = 245$ K. We note that the magnetic data are commensurate with the electronic transport results [Fig. 3(a)] and further support the ferroelastic-strain-induced conversion of the FMM phase into the PMI phase. Our findings demonstrate that the in-plane lattice strain produced by the ferroelastic domain switching of the PMN-PT substrates exhibits a great capability to manipulate the magnetic properties of the deposited films.

IV. CONCLUSIONS

In summary, we realize the strain-mediated nonvolatile ferroelastic control of the electronic transport and magnetic

properties in the LCMO/PMN-PT heterostructures and achieve a substantial strain tunability of resistivity and magnetization by 183 and 1768 in the vicinity of T_C, respectively. These lattice-coupled order parameters can be *in situ* reversibly manipulated via two stable and switchable in-plane strain states of the PMN-PT substrates, which is deeply associated with the intermediate state during domain switching near the coercive field. Moreover, the magnetically tunable strain effect, together with the strain-controlled MR effect, reveals the strong mutual interaction between the ferroelastic strain and the magnetic field, which can be reasonably interpreted in terms of the EPS model. Our findings provide a framework for understanding the evolution dynamics of the EPS against lattice strain and magnetic field, and designing the next-generation energy-efficient nonvolatile memory devices using domain-engineered ferroelastic switching.

[1] R. O. Cherifi, V. Ivanovskaya, L. C. Phillips, A. Zobelli, I. C. Infante, E. Jacquet, V. Garcia, S. Fusil1, P. R. Briddon, N. Guiblin, A. Mougin, A. A. Ünal, F. Kronast, S. Valencia, B. Dkhil, A. Barthélémy, and M. Bibes, Electric-field control of magnetic order above room temperature, Nat. Mater. **13**, 345 (2014).

[2] D. Pantel, S. Goetze, D. Hesse, and M. Alexe, Reversible electrical switching of spin polarization in multiferroic tunnel junctions, Nat. Mater. **11**, 289 (2012).

[3] H. J. A. Molegraaf, J. Hoffman, C. A. F. Vaz, S. Gariglio, D. van der Marel, C. H. Ahn, and J.-M. Triscone, Magneto-electric effects in complex oxides with competing ground states, Adv. Mater. **21**, 3470 (2009).

[4] C. A. F. Vaz, J. Hoffman, Y. Segal, J. W. Reiner, R. D. Grober, Z. Zhang, C. H. Ahn, and F. J. Walker, Origin of the Magnetoelectric Coupling effect in $Pb(Zr_{0.2}Ti_{0.8})O_3/La_{0.8}Sr_{0.2}MnO_3$ multiferroic heterostructures, Phys. Rev. Lett. **104**, 127202 (2010).

[5] S. Zhang *et al.*, Electric-Field Control of Nonvolatile Magnetization in $Co_{40}Fe_{40}B_{20}/Pb(Mg_{1/3}Nb_{2/3})_{0.7}Ti_{0.3}O_3$ Structure at Room Temperature, Phys. Rev. Lett. **108**, 137203 (2012).

[6] M. Liu, Z. Y. Zhou, T. X. Nan, B. M. Howe, G. J. Brown, and N. X. Sun, Voltage tuning of ferromagnetic resonance with bistable magnetization switching in energy-efficient magnetoelectric composites, Adv. Mater. **25**, 1435 (2013).

[7] M. Liu, B. M. Howe, L. Grazulis, K. Mahalingam, T. X. Nan, N. X. Sun, and G. J. Brown, Voltage-impulse-induced non-volatile ferroelastic switching of ferromagnetic resonance for reconfigurable magnetoelectric microwave devices, Adv. Mater. **25**, 4886 (2013).

[8] S. Finizio, M. Foerster, M. Buzzi, B. Krüger, M. Jourdan, C. A. F. Vaz, J. Hockel, T. Miyawaki, A. Tkach, S. Valencia, F. Kronast, G. P. Carman, F. Nolting, and M. Kläui, Magnetic Anisotropy Engineering in Thin Film Ni Nanostructures by Magnetoelastic Coupling, Phys. Rev. Applied **1**, 021001 (2014).

[9] T. X. Nan, Z. Y. Zhou, J. Lou, M. Liu, X. Yang, Y. Gao, S. Rand, and N. X. Sun, Voltage impulse induced bistable magnetization switching in multiferroic heterostructures, Appl. Phys. Lett. **100**, 132409 (2012).

[10] R. Schmidt, Investigation of the electronic structure of the charge-ordered phase in epitaxial and polycrystalline $La_{1-x}Ca_xMnO_3$ ($x = 0.55$, 0.67) perovskite manganites, Phys. Rev. B **77**, 205101 (2008).

[11] A. Biswas, M. Rajeswari, R. C. Srivastava, T. Venkatesan, R. L. Greene, Q. Lu, A. L. de Lozanne, and A. J. Millis, Strain-driven charge-ordered state in $La_{0.67}Ca_{0.33}MnO_3$, Phys. Rev. B **63**, 184424 (2001).

[12] M. Zheng, M. M. Yang, Q. X. Zhu, X. Y. Li, G. Y. Gao, R. K. Zheng, Y. Wang, X. M. Li, X. Shi, H. S. Luo, and X. G. Li, Tunable interface strain coupling and its impact on the electronic transport and magnetic properties of $La_{0.5}Ca_{0.5}MnO_3/Pb(In_{1/2}Nb_{1/2})O_3$-$Pb(Mg_{1/3}Nb_{2/3})O_3$-$PbTiO_3$ multiferroic heterostructures, Phys. Rev. B **90**, 224420 (2014).

[13] T. Wu, S. B. Ogale, S. R. Shinde, A. Biswas, T. Polletto, R. L. Greene, T. Venkatesan, and A. J. Millis, Substrate induced strain effects in epitaxial $La_{0.67-x}Pr_xCa_{0.33}MnO_3$ thin films, J. Appl. Phys. **93**, 5507 (2003).

[14] Y. H. Sun, Y. G. Zhao, H. F. Tian, C. M. Xiong, B. T. Xie, M. H. Zhu, S. Park, W. D. Wu, J. Q. Li, and Q. Li, Electric and magnetic modulation of fully strained dead layers in $La_{0.67}Sr_{0.33}MnO_3$ films, Phys. Rev. B **78**, 024412 (2008).

[15] D. N. Argyriou, U. Ruett, C. P. Adams, J. W. Lynn, and J. F. Mitchell, Phase separation in $Pr_{0.7}Ca_{0.3}MnO_{0.3}$: A case of weak quenched disorder, New J. Phys. **6**, 195 (2004).

[16] Z. G. Sheng, J. Gao, and Y. P. Sun, Coaction of electric field induced strain and polarization effects in $La_{0.7}Ca_{0.3}MnO_3/PMN$-PT structures, Phys. Rev. B **79**, 174437 (2009).

[17] S. Y. Wang and J. Gao, Modulation of metal-insulator transitions in $La_{0.8}Ca_{0.2}MnO_3/0.7Pb(Mg_{1/3}Nb_{2/3})O_3$-$0.3PbTiO_3$ heterostructures by electric fields, Europhys. Lett. **95**, 57001 (2011).

[18] R. K. Zheng, Y. Wang, J. Wang, K. S. Wong, H. L. W. Chan, C. L. Choy, and H. S. Luo, Tuning the electrical properties of $La_{0.75}Ca_{0.25}MnO_3$ thin films by ferroelectric polarization, ferroelectric-field effect, and converse piezoelectric effect, Phys. Rev. B **74**, 094427 (2006).

[19] T. Jiang, S. W. Yang, Y. K. Liu, Y. W. Yin, S. N. Dong, W. B. Zhao, and X. G. Li, Coaction and distinguishment of converse piezoelectric and field effects in $La_{0.7}Ca_{0.3}MnO_3/SrTiO_3/0.68Pb(Mg_{1/3}Nb_{2/3})O_3$-$0.32PbTiO_3$ heterostructures, Appl. Phys. Lett. **103**, 053504 (2013).

[20] Q. X. Zhu, W. Wang, S. W. Yang, X. M. Li, Y. Wang, H.-U. Habermeier, H. S. Luo, H. L. W. Chan, X. G. Li, and R. K. Zheng, Coaction and competition between the ferroelectric field effect and the strain effect in $Pr_{0.5}Ca_{0.5}MnO_3$film/$0.67Pb(Mg_{1/3}Nb_{2/3})O_3$-$0.33PbTiO_3$ crystal heterostructures, Appl. Phys. Lett. **101**, 172906 (2012).

[21] M. Liu, J. Hoffman, J. Wang, J. X. Zhang, B. Nelson-Cheeseman, and A. Bhattacharya, Non-volatile ferroelastic switching of the Verwey transition and resistivity of epitaxial Fe_3O_4/PMN-PT (011), Sci. Rep. **3,** 1876 (2013).

[22] M. M. Yang, X. Q. Zhao, J. Wang, Q. X. Zhu, J. X. Zhang, X. M. Li, H. S. Luo, X. G. Li, and R. K. Zheng, Intrinsic and quantitative effects of in-plane strain on ferroelectric properties of Mn-doped $BiFeO_3$ epitaxial films by *in situ* inducing strain in substrates, Appl. Phys. Lett. **104,** 052902 (2014).

[23] B. W. Zhi, G. Y. Gao, H. R. Xu, F. Chen, X. L. Tan, P. F. Chen, L. F. Wang, and W. B. Wu, Electric-field-modulated nonvolatile resistance switching in VO_2/PMN-PT(111) heterostructures, ACS Appl. Mater. Interfaces **6,** 4603 (2014).

[24] T. Wu, A. Bur, P. Zhao, K. P. Mohanchandra, K. Wong, K. L. Wang, C. S. Lynch, and G. P. Carman, Giant electric-field-induced reversible and permanent magnetization reorientation on magnetoelectric Ni/(011) $[Pb(Mg_{1/3}Nb_{2/3})O_3]_{(1-x)}$-$[PbTiO_3]_x$ heterostructure, Appl. Phys. Lett. **98,** 012504 (2011).

[25] T. Wu, P. Zhao, M. Bao, A. Bur, J. L. Hockel, K. Wong, K. P. Mohanchandra, C. S. Lynch, and G. P. Carman, Domain engineered switchable strain states in ferroelectric (011) $[Pb(Mg_{1/3}Nb_{2/3})O_3]_{(1-x)}$-$[PbTiO_3]_x$ (PMN-PT, $x \approx 0.32$) single crystals, J. Appl. Phys. **109,** 124101 (2011).

[26] M. Zheng, Q. X. Zhu, X. Y. Li, M. M. Yang, Y. Wang, X. M. Li, X. Shi, H. S. Luo, and R. K. Zheng, Electric-field-controlled interface strain coupling and non-volatile resistance switching of $La_{1-x}Ba_xMnO_3$ thin films epitaxially grown on relaxor-based ferroelectric single crystals, J. Appl. Phys. **116,** 113911 (2014).

[27] See Supplemental Material at http://link.aps.org/supplemental/10.1103/PhysRevApplied.5.044002 for Figs. S1, S2, and Table I.

[28] Y. M. Xiong, G. Y. Wang, X. G. Luo, C. H. Wang, X. H. Chen, X. Chen, and C. L. Chen, Magnetotransport properties in $La_{1-x}Ca_xMnO_3$ ($x = 0.33$, 0.5) thin films deposited on different substrates, J. Appl. Phys. **97,** 083909 (2005).

[29] N. D. Mathur, M.-H. Jo, J. E. Evetts, and M. G. Blamire, Magnetic anisotropy of thin film $La_{0.7}Ca_{0.3}MnO_3$ on untwinned paramagnetic $NdGaO_3$ (001), J. Appl. Phys. **89,** 3388 (2001).

[30] T. X. Nan, M. Liu, W. Ren, Z. G. Ye, and N. X. Sun, Voltage control of metal-insulator transition and non-volatile ferroelastic switching of resistance in VO_x/PMN-PT heterostructures, Sci. Rep. **4,** 5931 (2014).

[31] Y. F. Lu, J. Klein, C. Höfener, B. Wiedenhorst, J. B. Philipp, F. Herbstritt, A. Marx, L. Alff, and R. Gross, Magnetoresistance of coherently strained $La_{2/3}Ba_{1/3}MnO_3$/$SrTiO_3$ superlattice, Phys. Rev. B **62,** 15806 (2000).

[32] C. Thiele, K. Dörr, S. Fähler, L. Schultz, D. C. Meyer, A. A. Levin, and P. Paufler, Voltage-controlled epitaxial strain in $La_{0.7}Sr_{0.3}MnO_3$/$Pb(Mg_{1/3}Nb_{2/3})O_3$-$PbTiO_3$(001) films, Appl. Phys. Lett. **87,** 262502 (2005).

[33] S. L. Yuan, Z. Y. Li, W. Y. Zhao, G. Li, Y. Jiang, X. Y. Zeng, Y. P. Yang, G. Q. Zhang, F. Tu, C. Q. Tang, and S. Z. Jin, Phenomenological model for colossal magnetoresistance in optimally doped manganese perovskites, Phys. Rev. B **63,** 172415 (2001).

[34] M. Copel, M. A. Kuroda, M. S. Gordon, X.-H. Liu, S. S. Mahajan, G. J. Martyna, N. Moumen, C. Armstrong, S. M. Rossnagel, T. M. Shaw, P. M. Solomon, T. N. Theis, J. J. Yurkas, Y. Zhu, and D. M. Newns, Giant piezoresistive on/off ratios in rare-earth chalcogenide thin films enabling nanomechanical switching, Nano Lett. **13,** 4650 (2013).